Calibration Report of the EFW Measurements in the Cluster Active Archive (CAA)

prepared by

Yuri Khotyaintsev

Table of Contents

1 Introduction

This document describes calibration results and procedures of the CAA products from the EFW instrument.

2 Instrument Description

A detailed description of the EFW instrument can be found in *Gustafsson et al*. (1997). We first briefly describe the raw quantities measured by the instrument which correspond to Level 1 products in the CAA. The detector of the instrument consists of four spherical sensors numbered 1 to 4 deployed orthogonally on 44 meter long wire booms in the spin plane of the spacecraft as illustrated in Figure 1. The potential drop between two sensors, separated by 88

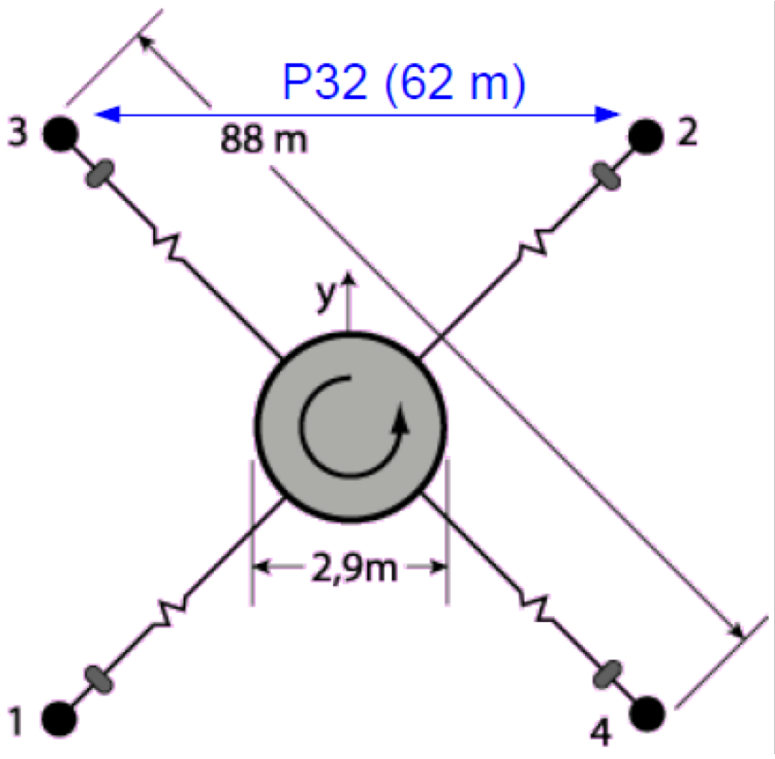

Figure 1: The EFW experiment

m tip-tip (62 m in case of P32) is measured to provide an electric field measurement (CAA quantities P12/P32 and P34). The probe difference signals are normally routed through 10

Hz low-pass filters if sampled at 25 s^{-1}, and through 180 Hz low-pass filters when sampled at 450 s^{-1} (see "EFW non-standard operations dataset" in Section 9 for the exceptions). The potential difference between each sensor and the spacecraft (CAA quantities P1, P2, P3 and P4) is measured separately with a sampling frequency of 5 s^{-1} after routing through low-pass filters with a cut-off frequency of 10 Hz.

The EFW instrument measures the electric field only in the spacecraft spin plane, therefore a spin-plane oriented coordinate system is best suited for scientific studies involving the electric field. The **ISR2** (Inverted Spin Reference) system, also known as **DSI** (Despun System Inverted), is such a system. The X and Y axes are in the spin plane, with X pointing as near sunward as possible and Y perpendicular to the sunward direction, positive towards dusk. The Z-axis is along the (negative) spacecraft spin axis, towards the north ecliptic. The coordinate system is called "Inverted" because the actual spin axis of Cluster is pointing towards the south ecliptic. The difference between ISR2 (DSI) and the GSE (Geocentric Solar Ecliptic) is a tilt of 2 to 7 degrees of the Z-axis performed in order to avoid shading of the EFW probes by the spacecraft. The exception is the May 2008 "tilt campaign" when the tilt angle on C3 can be up to 45 degrees.

3 Measurement Calibration Procedures

Spacecraft potential data (probe-to-spacecraft, not the plasma-to-spacecraft potential see *Cully et al. 2007*) in the CAA does not require any special calibration. L2_P is usually computed as average of all four probes; if one or two probes are missing, it is calculated as average of two opposing probes, or only one if these probes are non-opposing. If only one probe is available L2_P is given by the potential of that probe. In case of probe saturation due to high bias current (see "Detection of saturation due to high bias current in dense plasmas" in Section 9), we switch from the averaging to using maximum of all available probes, which gives the best estimate of the spacecraft potential in this case.

Here we describe the processing chain of the electric field data. At the initial stage of production we remove intervals with: bad data due to issues with electronics, probe saturations due to low plasma density, and non-optimal bias current settings. Usually, only a few minutes of data are removed from each orbit for these reasons. However, large data gaps may occasionally occur. If the spacecraft is in the solar wind we attempt to correct for the

wakes usually present in the raw data (see “Cleaning wakes in the solar wind”).

3.1 Spin fitting

In the presence of a constant ambient electric field, the raw data signal (probe potential difference) is a sine wave where the amplitude and phase give the electric field magnitude and direction. A *least-squares fit* to the raw data of the form

$$y = \boldsymbol{A} + \boldsymbol{B}\sin(\omega t) + \boldsymbol{C}\cos(\omega t) + \boldsymbol{D}\sin(2\omega t) + \boldsymbol{E}\cos(2\omega t) + \ldots \qquad (1)$$

is done once every 4 seconds ($2\pi/\omega \approx 4$ sec is the spacecraft spin period), and gives the following output:

- The sine and cosine terms, ***B*** and ***C*** (L3_SFIT dataset) are used to compute the 4-sec-resolution electric field in ISR2.
- The *raw data DC offset*, ***A***. Ideally, the DC level of the raw data should be zero, however small differences between the probe surfaces and in the electronics create a DC offset in the raw data. If not corrected, it shows up as a signal at the spin frequency in the despun electric field. The DER dataset is based on ***A*** (see section 6).
- The standard deviation of the raw data from the fitted sine wave (L3_E dataset).
- Higher order terms, ***D***, ***E***, ..., may be used for diagnostics of data quality (not delivered to the CAA).

The electric field (computed from ***B*** and ***C*** for one of the probe pairs) and the standard deviation are available in the CAA as Level 3 E.

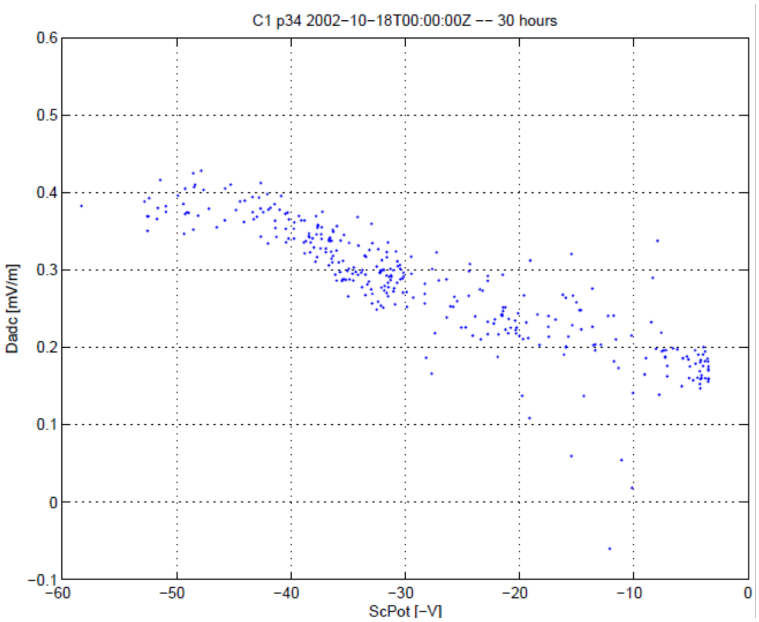

Figure 2: Raw data DC offset vs spacecraft potential

3.2 Raw data DC offset

The raw data DC offset (***A***) from both probe pairs is used for processing the full-resolution (L2) data. It is applied to P12/P32 and P34 prior to despinning and available in the CAA as L3_DER product. Variations in the electric field cause small changes of the DC offset. DC offset also depends on the surrounding plasma environment as illustrated in Figure 2. Therefore we want a smoothened value and at the same time to track changes in the plasma environment, that is why the DC offset is smoothed using a weighted average over 7 spins using weights [.07 .15 .18 .2 .18 .15 .07] (see the ICD). The smoothed offset is delivered to the CAA as the DER dataset. Intervals containing WHISPER pulses are blanked prior to despinning.

3.3 Delta offset

Another offset which is applied during despinning is the so called Delta offset, which is based on the difference between the electric fields in ISR2 obtained from the least-squares fit procedure for individual probe pairs, P12/P32 and P34. This offset comes from differences in the probe characteristics which evolve with time. Evolution of delta offsets for Cluster 2 for 2001-2005 is shown in Figure 3. The spikes in the plot are usually due to one of the probe pairs being partially saturated (removed during the computation of the offset). To get rid of these spikes and also knowing that evolution of the offset is very slow, we use a median value over a 6 day period corresponding to approximately 3 orbits (shown in green). The blue curve shows values of the offset computed over 90-min (NM) or 30-min (BM1) intervals. On rare occasions when the delta offset changes rapidly, as for example after some of the

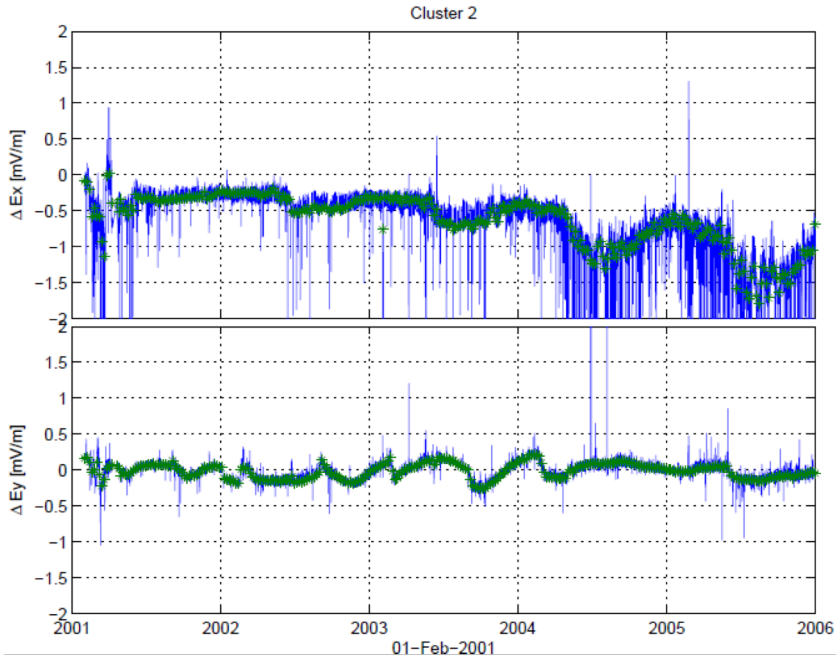

Figure 3: Delta offsets for Cluster 2

maneouvres, we use manually verified tabulated values. The delta offset is applied during the despin when L2_E is produced. The delta offset is always corrected on P12/32. The value applied is given in FILE_CAVEATS section of the CEF file:

```
ENTRY        =    "2007-12-02T00:00:00.000Z/2007-12-02T01:09:00.000Z
p12 offset (ISR2): dEx=0.21 dEy=-0.05"
```

3.4 Amplitude correction

At this stage both the full-resolution (L2, from despinning) and 4-sec (L3, from least-squares fit) electric fields contain systematic errors, namely an amplitude factor and a DC offset, which need to be corrected for.

The ambient electric field is "short-circuited" by the presence of the spacecraft and wire booms. This is caused by the spacecraft potential, which is also the potential of the wire booms, extending out to a large distance from the spacecraft. On the basis of simulations and comparisons with other Cluster instruments it has been determined that the measured electric field magnitude needs to be multiplied by a factor of 1.1 (see "ISR2 offsets and Amplitude correction factor" in Section 6.1 for more detail) to get the real electric field (see also *Cully et al. 2007*). However, this factor depends on the plasma environment, and in some cases may deviate from the value used. In case of Cluster it can vary in a range from 1.0 to ~1.2, but is usually 1.1.

3.5 ISR2 DC offset

The spacecraft, wire booms and probes emit photoelectrons, which create an excess of negative charge on the sunward side. This will be measured by the EFW instrument as a spurious sunward electric field, generally referred to as the sunward DC offset. Most of time the offset varies slowly with time and plasma conditions around the spacecraft, and is slightly different for the different spacecraft. However, fast changes can also occur related to for example fast crossings of plasma boundaries or rapidly varying solar UV flux that both can cause changes in the satellite photoelectron cloud.

The magnitude of the offset is determined by comparisons with other measurements, performed by Electron Drift Instrument (EDI) and Cluster Ion Spectrometry experiment (CIS). The values of the offsets that have been subtracted from the data in the CAA are given in the FILE_CAVEATS section of the CEF files. The photoelectron asymmetry responsible for the sunward DC offset by definition gives an offset in the sunward direction only. However, results of comparisons with other instruments have at times shown an offset of a fraction of mV/m also in the duskward direction, which is not yet well understood. In most cases the duskward offset is negligible.

Prior to delivery to the CAA we attempt to identify and mark intervals with suspected spurious fields in various magnetospheric regions (see "Detection of spurious electric fields

in the plasmasphere" and "Detection of cold ion flow wakes" in Section 9).

4 Measurement Processing Procedures

4.1 Issues due to electronics & instrument saturations

In this chapter we describe procedure we use to identify bad data due to issues with electronics. These include instrument misconfiguration, malfunction, digital saturation, etc. Data during such intervals cannot be recovered.

First we remove all data during the interval 1 minute prior (the timing of such data is unknown) and 3 minutes after the EFW reset. Following the reset EFW boots into default mode which has non optimal bias current settings. These settings are usually reprogrammed to nominal 2-3 minutes after a reset.

After this we check the actual bias current measurements and disregard all data which have non-nominal settings. Nominal bias current setting for all years of operation can be found in "EFW standard operations database" (https://cluster.irfu.se/efw/ops/#standard) and actual bias current settings are included in the HK dataset.

Then we check for probe saturations. First we look for probes and probe pairs "getting stuck" which is identified by a non-changing measurement for four consecutive points. Then we check for measurements being saturated due to low density when the probes reach the maximum digital value of 68 V.

Some additional intervals may be disregarded manually on the basis of the "EFW non-standard operations database" (https://cluster.irfu.se/efw/ops/ns_ops.html). These usually include maneuvres, bad telemetry packets, unusual sampling modes and instrument settings. These intervals are marked in the quality information supplied with the electric field data: bits 0-6 set in the E_bitmask (see CAA-EFW User Guide). For such intervals the data will typically contain the fill value or there will be a data gap.

4.2 Detection of saturation due to high bias current in dense plasmas

Due to long term evolution of probe characteristics the nominal bias current setting of 140 nA started to cause saturations in the dense magnetosheath plasmas in spring 2004. The problem became more prominent in 2005 and the nominal setting was lowered to 100 nA. See "EFW standard operations database" for more details. The saturated time intervals usually contain very large electric field spikes in every spin with amplitudes sometimes reaching the digital saturation level. We have developed an algorithm which detects such saturations based on the amplitude of the spikes, their shape, etc. The algorithm is in many ways similar to the one used for detection of solar wind wakes. The algorithm in action is illustrated in Figure 4. The time intervals for which the saturation was found are marked by red/green envelope. The saturated time intervals are blanked in the CAA, as they usually contain useless measurements. These intervals are marked in the quality information supplied with the electric field data: bit 14 set in the E_bitmask (see the CAA-EFW User Guide).

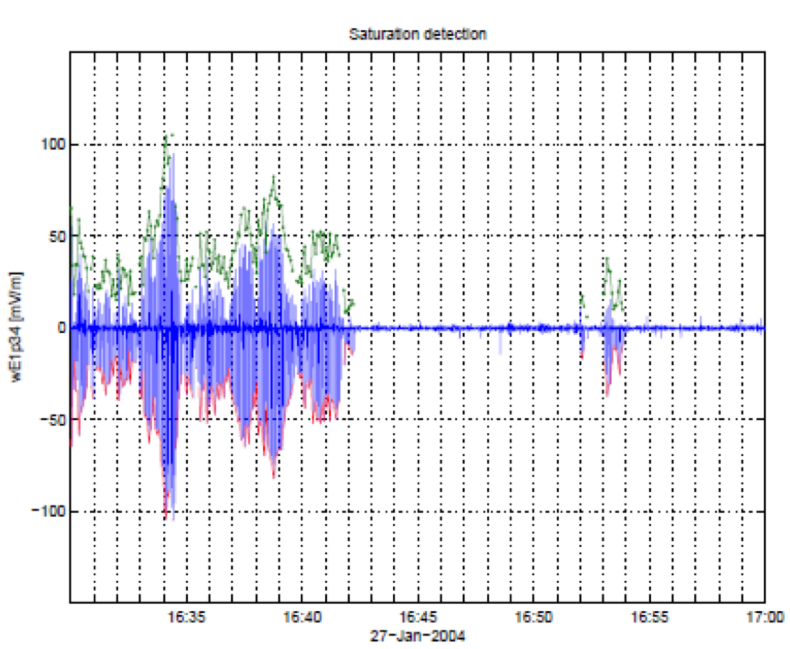

Figure 4: Detection of saturated intervals due to high bias current.

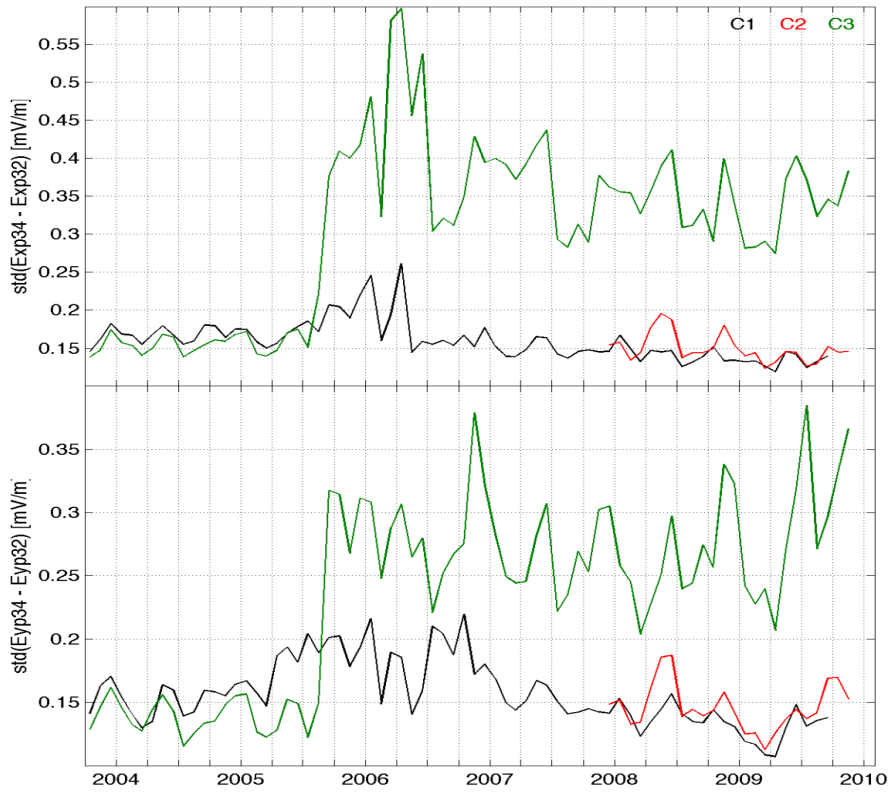

Figure 5: Difference between the spin fits from the long (p34 – 88m) and short asymmetric (p32 – 62m) probe pairs.

4.3 Measurements with asymmetric probe configuration

In order to measure full resolution electric fields by EFW two probe pairs are required. The optimal situation is when the probe pairs are equally long, orthogonal and symmetric with respect to the spacecraft. The spacecraft on which probe 1 failed after some period of operations (for exact times see "EFW non-standard operations database") are normally run in so called "*asymmetric mode*", e.g. difference between probe pairs 2 and 3 is measured in addition to p34. Then p12 can be computed (on ground) from a combination of p32 and p34 and normal processing procedure can be used.

However this measurement has a lower quality compared to "normal" p12 because p32 is shorter (62 m instead of 88 m) and it is not symmetric with respect to the spacecraft. The spin fit data is practically not affected by this problem. Figure 5 shows the standard deviation

of the difference between the spin resolution electric fields obtained from the long p34 and the short p32 probe pairs. Here we have included data only from spacecraft spins with relatively quiet electric activity, i.e. when the standard deviation of the spin fit is below 0.3. One can see that statistical difference between the spin fits from the long and short probe pairs is small, typically about 0.15 mV/m for C1 and C2, as well as for C3 before September 2005. Since September 2005 something happened to C3, and it shows reduced data quality.

For the full resolution electric field, using the short probe pair results in modulation at 2 times the spin frequency in the raw data, which results in signals at 1 and 3 times the spin frequency (about 0.25 and 0.75 Hz) in the despun data (see upper panel in Figure 6). This

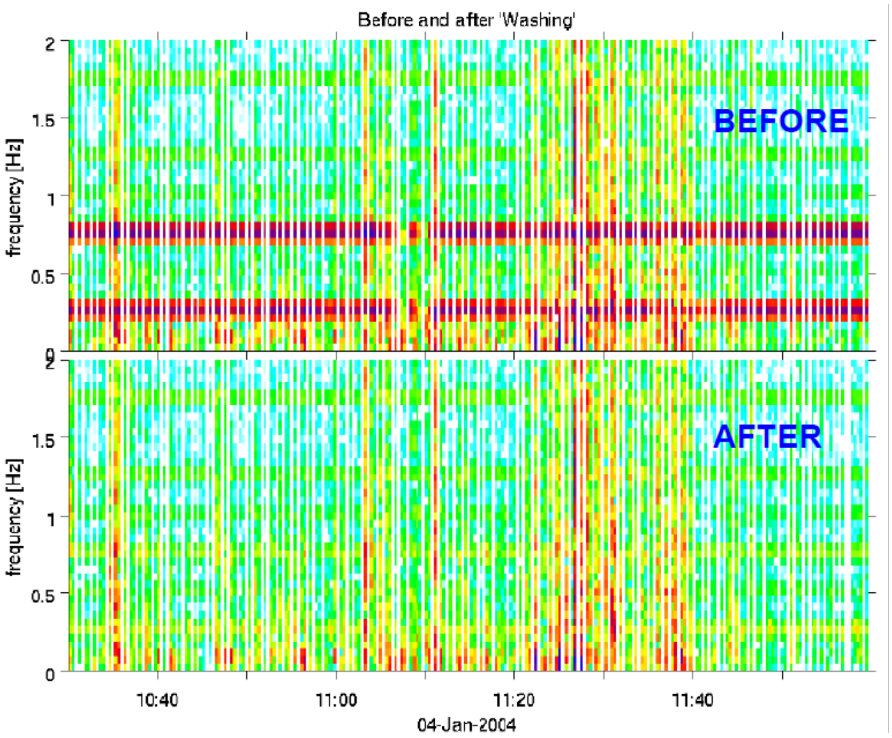

Figure 6: Original and "washed" data in the asymmetric configuration

modulation becomes apparently prominent when electric fields become small.

We have tried two algorithms for cleaning (we use term “washing”) this modulation in the data. First algorithm, referred as “old”, was making FFT of the p32 data, removing the peak at 2 times the spin frequency by interpolating the spectrum and then doing inverse FFT. The results from this method were good but not satisfactory, moreover they were creating

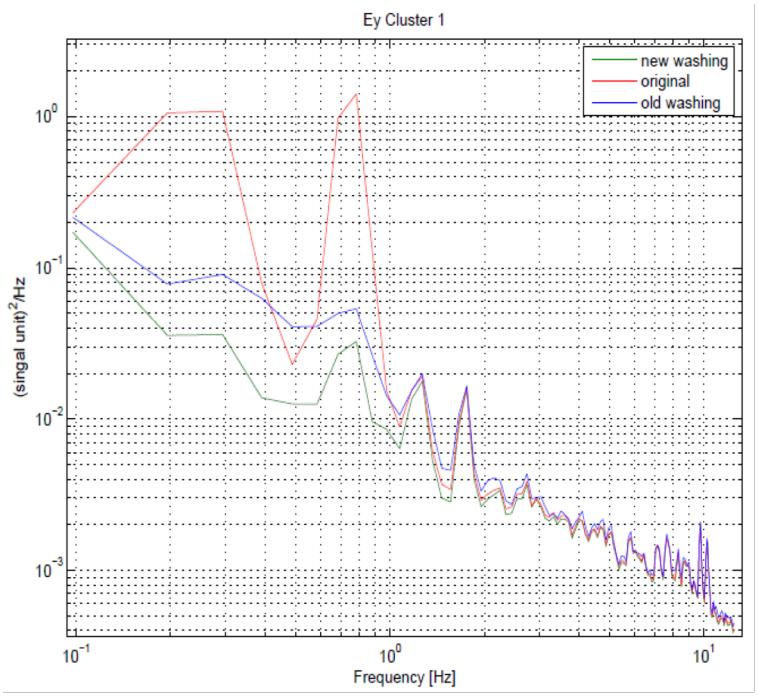

Figure 7: E spectrum before and after washing. The spacecraft spin frequency is ~0.25 Hz.

problems at boundaries of the FFT window. That is why we developed a new algorithm, referred as “new”, which is simply removing the signal at 2 times the spin frequency obtained from spin fitting (terms ***D*** and ***E*** in Equation 1). The spectra and time series resulting from these two algorithms are illustrated in Figures 7 and 8.

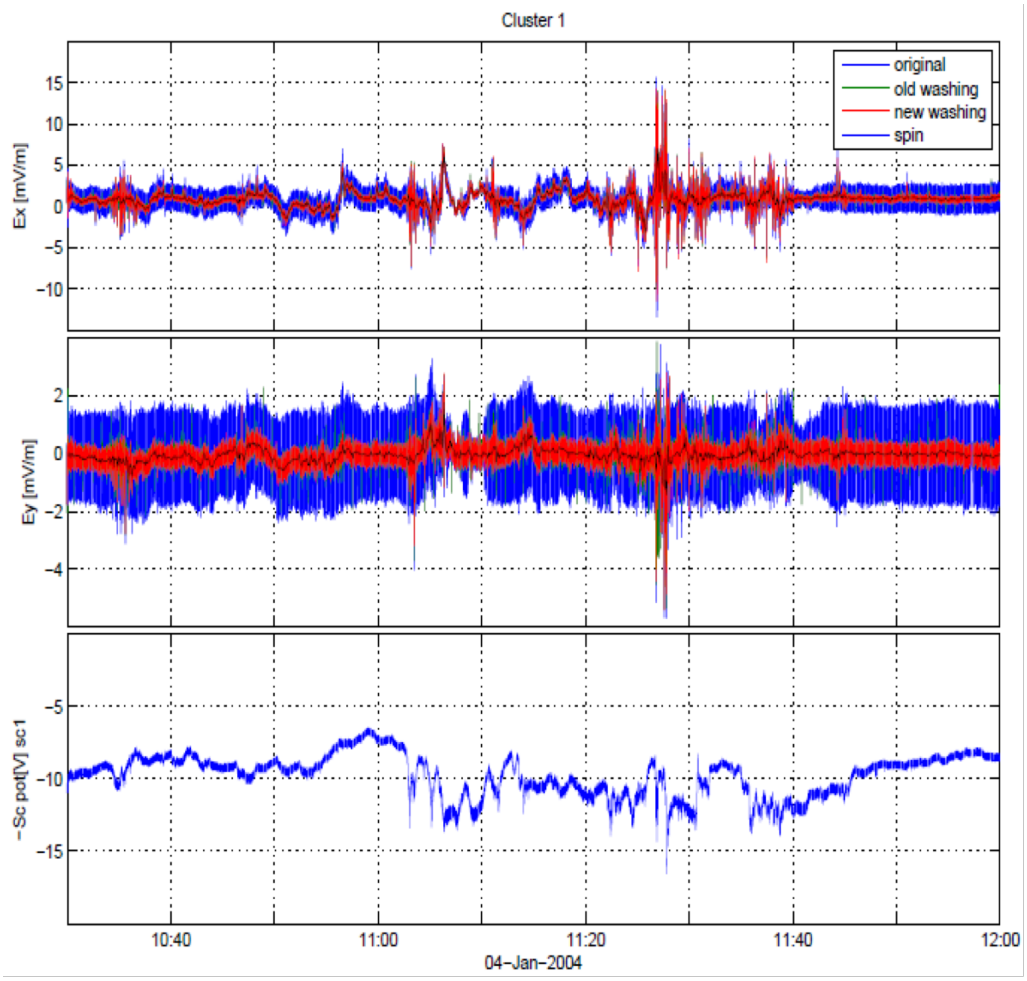

Figure 8: Timeseries of the despun electric field resulting from raw and washed data.

4.4 Cleaning wakes in the solar wind

In the solar wind we remove wakes. Detailed description of the procedure can be found in

Eriksson et. al. 2007. Wakes are routinely removed in the solar wind and the affected spins have bit 10 set in the E_bitmask for the electric field datasets (see the CAA-EFW User Guide). This is done before the spin fitting procedure.

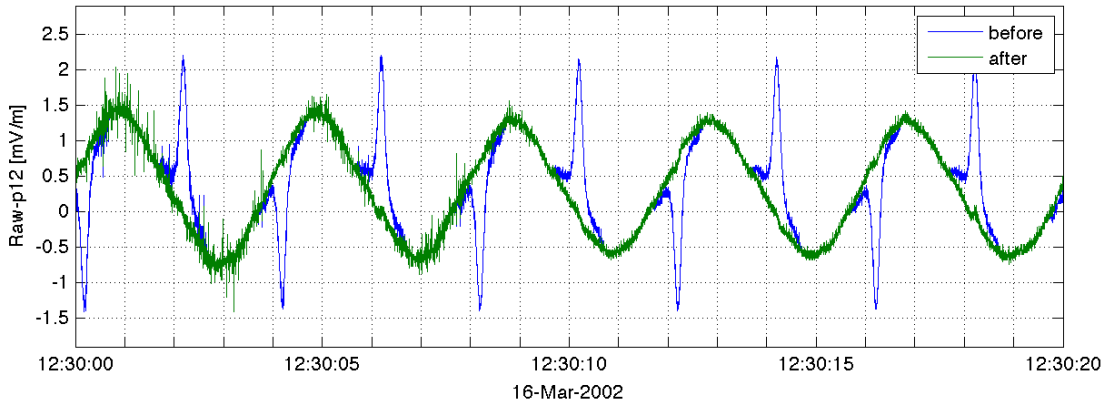

Figure 9: Solar wind wake removal.

4.5 Detection of spurious electric fields in the plasmasphere

During comparisons of electric field measurements made by EFW and EDI in the inner magnetosphere, it was found that EFW sometimes measures a spurious field of the order of 1-2 mV/m, mostly in the sunward direction (Figure 10, see also Figure 1c in *Puhl-Quinn et al. 2008*). The raw data signal is often non-sinusoidal (top panel). This problem is not quantitatively understood, but apparently depends on simultaneously acting phenomena:

(a) the dense plasmaspheric plasma can sometimes be so high as to give a random electron current to the probes almost as large as the applied bias current, driving the probe away from its vacuum potential with respect to the plasma;

(b) the wake created by the spacecraft makes the random current and the resulting error dependent on the spin phase and hence gives an apparent DC field in a non-spinning reference frame; and

(c) small differences in probe surfaces and bias circuitry will make this effect slightly different between the probes, further complicating the result.

A first principles error treatment is therefore complex. Nevertheless, an empirical algorithm has been developed to detect the bad data. We have developed an algorithm to detect such spurious fields by comparing the electric field measured by EFW to corotation electric field. If 1 minute averaged measured field deviates from corotation by more than 1 mV/m, such interval will be marked as "plasmaspheric wake" in the quality information supplied with electric field data. This Algorithm is applied only for altitudes below 6 R_E and when negative of the spacecraft potential exceeds -1.5 V, e.g. really only in very dense corotating

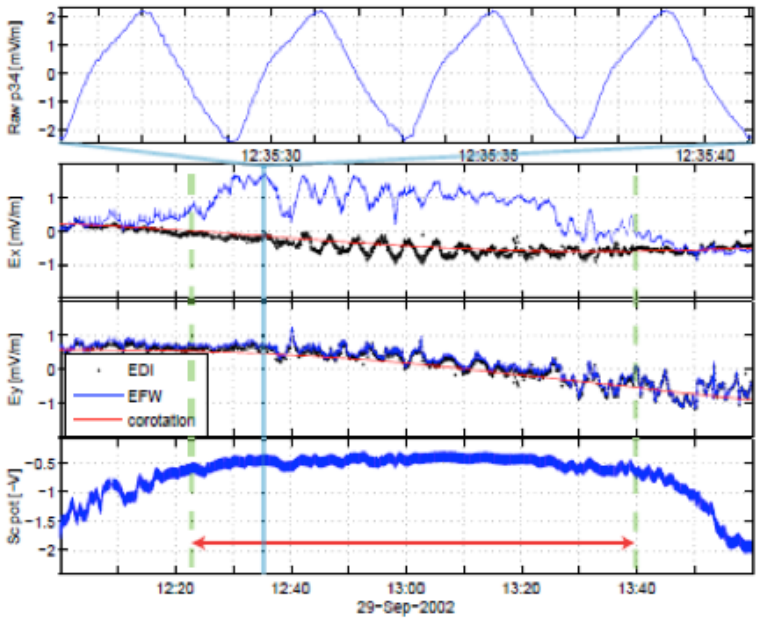

Figure 10: Spurious fields in the plasmasphere

plasmasphere. We need compare to corotation because the EDI measurements are not always available and never on C4. The algorithm in action is illustrated in Figure 10. The panes show ISR2 components of electric fields measured by EFW, EDI and also the corotation fields. The upper panel shows large deviation of EFW Ex from both the corotation and EDI measurement, and such data interval will be marked as "wake" in the quality data, bit 12 set in the E_bitmask for the electric field datasets (see the CAA-EFW User Guide). One should note that the spurious field may appear also in ISR2 Y direction.

4.6 Detection of cold ion flow wakes

One of the most problematic regions for measuring electric fields with double probe instruments (as EFW) are regions with low plasma density and flowing cold plasmas. In the low-density plasma encountered for example in the tail lobes, above the polar caps and in the

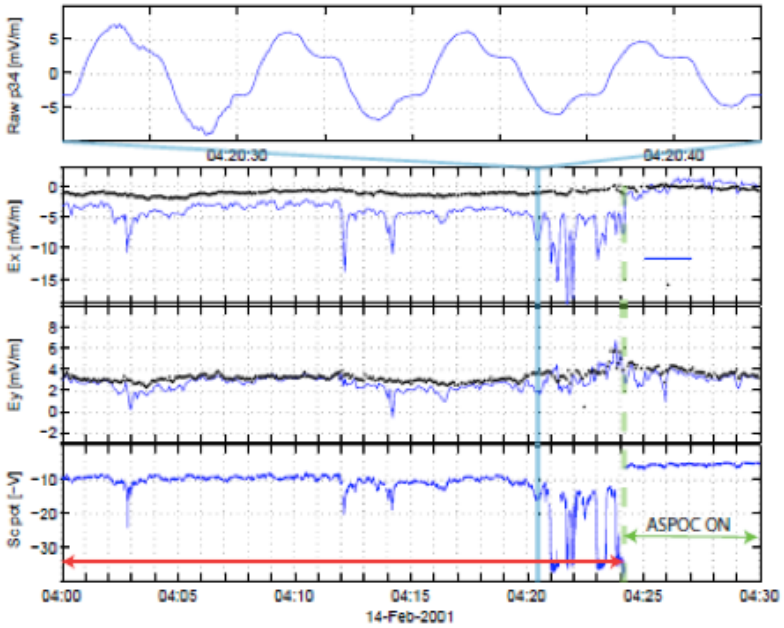

Figure 11: Wake detection in low density plasmas (EFW-blue, EDI-black).

low latitude dayside magnetosphere the spacecraft potential is usually of the order of several tens of volts. A cold ion population flowing in such plasma environments will see effectively much thicker booms (several meters instead of a few mm), creating a large negatively charged wake behind the booms in the direction of flow (*Eriksson et al. 2006, Engwall et al. 2006*).

Figure 11 shows an example of such a wake, defined by a large deviation of E_x measured by the EFW and EDI. When ASPOC is operating, the spacecraft potential is kept at a much lower value and the problem of wakes due to cold ion drift is much less severe. In comparison to the solar wind wake the ion drift wake is broader and more diffuse. For a relatively small wake the raw data are non-sinusoidal (see top panel in Figure 11). For a large wake they can become sinusoidal again and look very similar to those created by a real ambient electric field.

The CAA production software attempts to detect such ion wakes by looking at a combination of parameters, such as spacecraft potential, magnetic field direction, and the relation between different electric field components. For small magnetic field elevations (B direction is within 15 degrees from the spin plane) we check for the ratio between the components of E along the projection of B into the spin plane and perpendicular to it. For larger elevations we look at the ratio between the measured (spin plane) and unmeasured (perpendicular to the spin plane) components of $E_\perp$, where $E_\perp$ is computed under assumption of zero parallel electric field, $\mathbf{E}\cdot\mathbf{B} = 0$. Higher ratios indicate a higher probability of the wake being present in the data. At present there is no algorithm to correct the data, and the bad intervals are marked in the quality information supplied together with Level 2 and Level 3 data: bit 11 set in the E_bitmask (see CAA-EFW User Guide). Since it is sometimes difficult to discern between these wakes and a real electric field, analysis of the electric field should be done with caution in regions with possible cold ion drifts.

5 Results of Calibration Activities

Major calibration activities include determination of Raw Data Offset (L3_DER product) and Delta Offsets which are described in the previous section.

5.1 EFW noise and sensitivity

Here we describe sensitivity level and noise characteristics which can be expected from the EFW data. Figure 12 shows a typical spectrum of Ey ISR2 measured by EFW in the solar wind; in this example the E-field is sampled at 450 Hz (BM1) and then a low-pass filtered at 180 Hz. In the solar wind the electric field has one of the lowest signal levels comparing to all the regions encountered by Cluster and the EFW sensitivity level is often reached at frequencies above several Hz. We choose to study the Ey ISR2 component on C4, which is one of the cleanest signals EFW available on Cluster. The expected spectrum has a power-law

shape which corresponds to a straight line in a log-log plot. One can see that the measured spectrum is approximately a power-law at low frequencies and starts to flatten at several Hz, reaching the sensitivity floor of ~5*10-6 $(mV/m)^2/Hz$ at frequencies above 20 Hz.

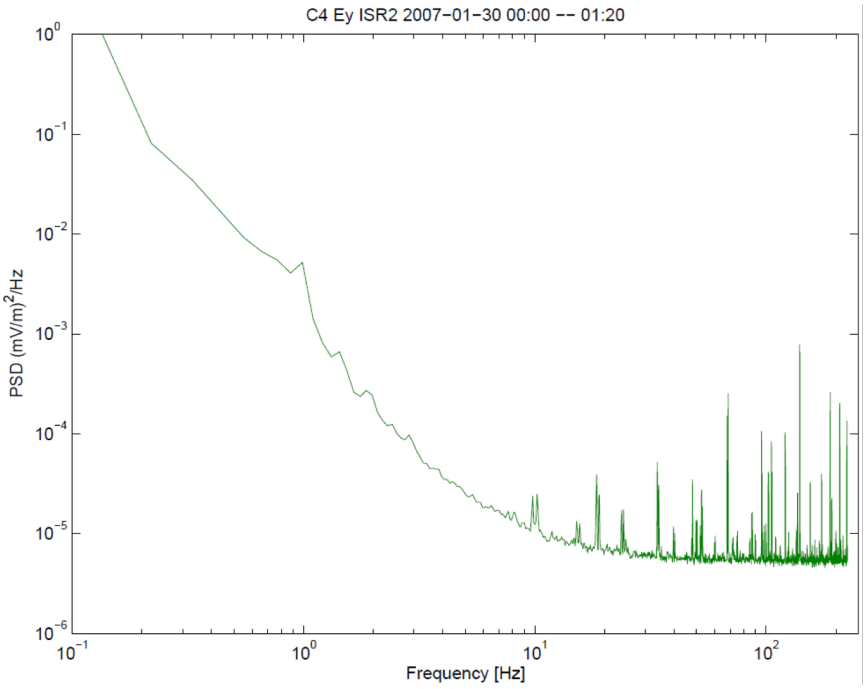

Figure 12: Ey spectrum in the solar wind.

Another striking feature which can be seen in Figure 12 is presence of sharp peaks at frequencies above 10 Hz. These peaks are coming from some high frequency signal inside the EFW electronics which is aliased down and are not affected by the 180 Hz low-pass filter.

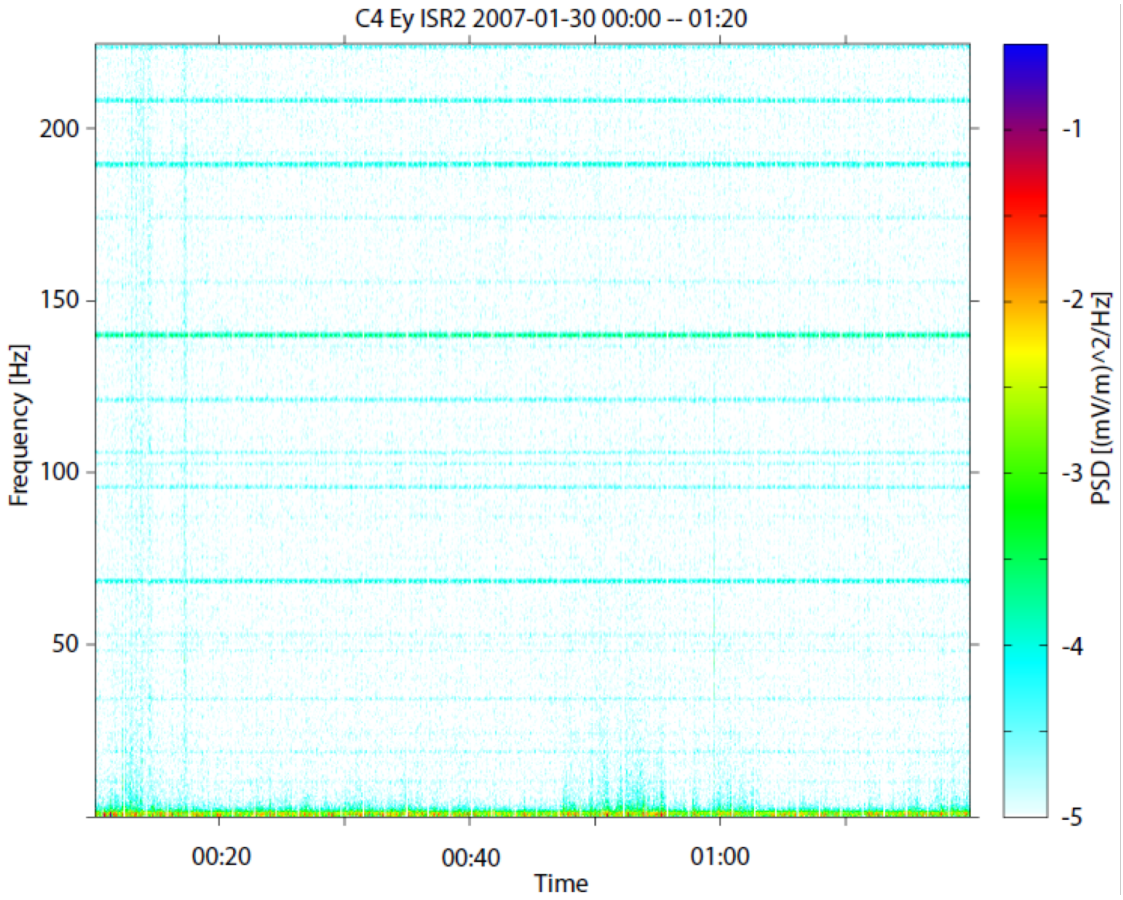

Figure 13: Time-frequency spectrogram of Ey in the SW

Figure 13 shows a time-frequency spectrogram of the same data and one can clearly see that the peaks in the spectrum are coming from the narrow spectral lines. In some cases it is possible to see a small frequency drift of these lines, which can be possibly attributed to heating/cooling of the electronic components when the spacecraft enters a plasma region with different properties. These lines could be in principle removed from the data, but it does not make much sense since the actual signal level is significantly below the sensitivity level in this case.

We have studied the sensitivity level of EFW by looking at the part of the spectrum between 70 and 180 Hz. The BM1 EFW data for 2001-2008 were split into 30 minute intervals, then a spectrum was computed over every 4 seconds of data, the spikes were thrown away and the the mean value was computed in 70-180 Hz range. Then we selected the lowest value in the 30 minute interval. The result for probe pair 12/32 all spacecraft are plotted in Figure 14. One can see that the sensitivity level is ~2*10-6 $(mV/m)^2/Hz$ at the beginning of the mission.

Then it increases by a factor 10-20 after probe 1 gets broken on C1, C3 and C2.

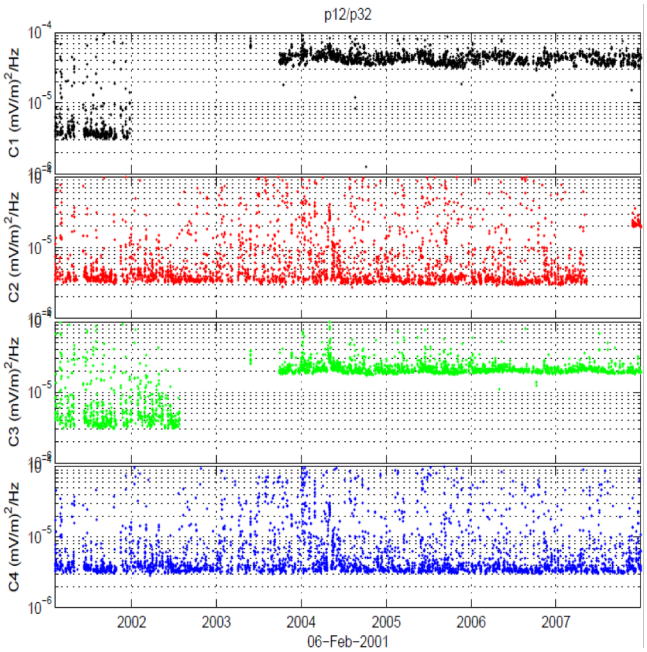

Figure 14: Evolution of sensitivity level on p12/p32

The results for probe pair 34 are shown in Figure 15. Here the initial level is about 5 times higher than for p12. The level gets slightly higher with introduction of the EFW flight software version 2.4 (FSW 2.4) in the end of 2003, where the analog difference is replaced by digital in order to compute p32.

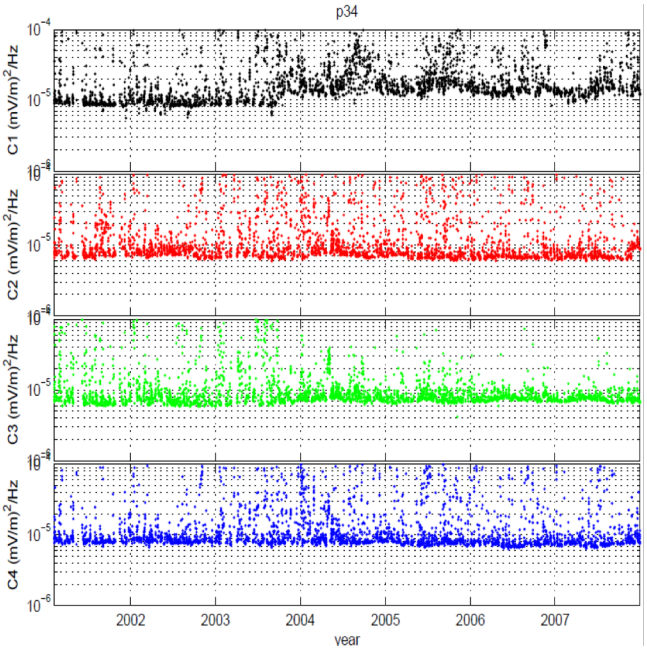

Figure 15: Evolution of sensitivity level on p34

6 Results of Cross-Calibration Activities

Cross calibration was mainly used to determine the amplitude correction factor for the electric field data and offsets in ISR2.

We have also performed a large "Cross-calibration study" in order to evaluate the quality of electric fields measured by different instruments.

6.1 ISR2 offsets and Amplitude correction factor

Our main assumption in the study of ISR2 offsets is that the offsets depend on the instrument configuration, spacecraft attitude and that the dependence on surrounding plasma parameters is weak, i.e. being in the same kind of plasma environment (for example plasmasheet) and having the same instrument settings and probe properties for two different time intervals, the difference for between ISR2 offsets for the two intervals must be within the uncertainty of the offset determination (several tenth of mV/m). As the offsets still depend on the plasma environment we decided to split the dataset into two groups "solar wind/magnetosheath" and "magnetosphere" which correspond to two situations with "cold

and dense" and "hot and rarefied" plasmas. To split every orbit into these two groups we have used the Shue magnetopause model (*Shue et al. 1997*) with realistic solar wind parameters measured by ACE.

6.1.1 Offsets in the solar wind and magnetosheath

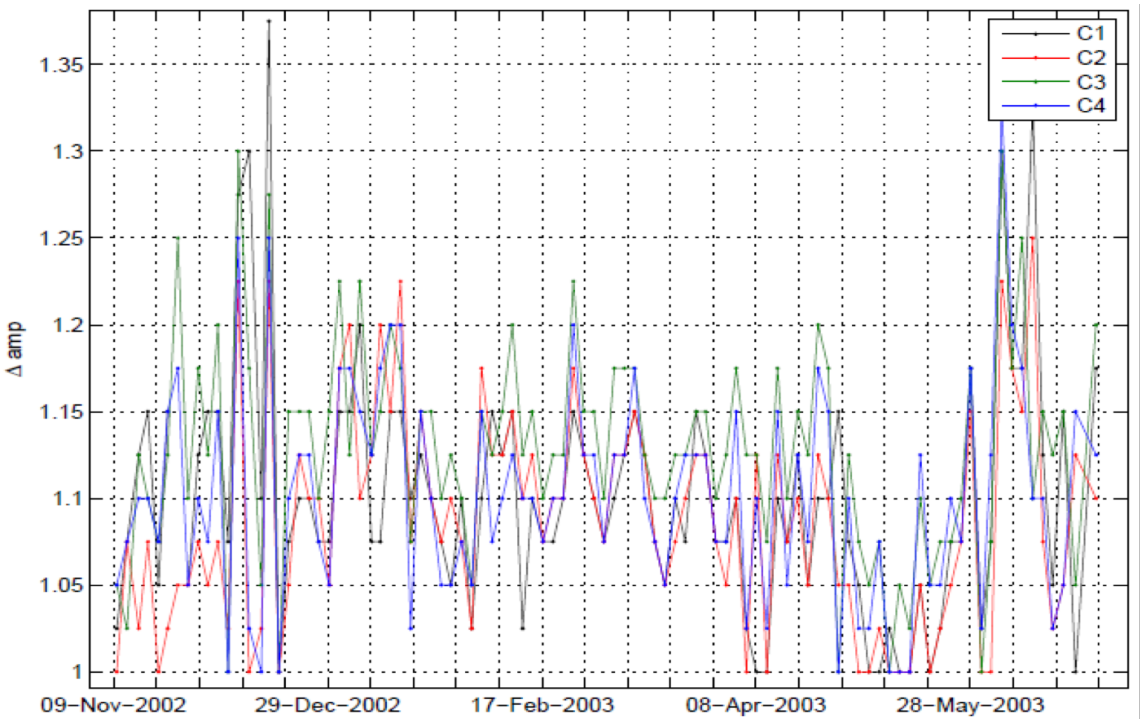

Figure 16: Amplitude correction factor in fall 2002 - spring 2003

6.1.1.1 Amplitude correction factor

First we studied the amplitude correction factor (see Section 3.4 , e.g. the factor by which the measured electric field amplitude needs to be increased in order to get the real electric field present in plasmas. The ambient electric field is "*short-circuited*" by the presence of the spacecraft and wire booms. This is caused by the spacecraft potential, which is also the potential of the wire booms, extending out to a large distance from the spacecraft.

We have used the ISR2 Y components of the electric field to determine the amplitude correction factor. This component of E is generally free from offsets and thus by comparing Ey from EFW and CIS-HIA we are able to deduce the amplitude correction factor. Results of such computations for the spring season of 2002 are shown in Figure 16. Every point in the plot corresponds to one orbit of data. One should mention that variations seen in the data are

not caused by changes in the factor, but rather by bad data and insufficient data coverage.

On the basis of simulations and comparisons with other Cluster instruments it has been determined that the measured electric field magnitude needs to be multiplied by a factor of 1.1. We use this constant value through the entire mission. It is given as a dAmp parameter in the FILE_CAVEATS section in the CEF files for the electric field data.

6.1.1.2 ISR2 offsets

After we know the amplitude correction factor we can determine the ISR2 offsets, which is simply a difference between the spin plane electric fields measured by EFW and CIS-HIA (VxB).

First, we perform the inter-spacecraft calibration under assumption that all the spacecraft observe the same large-scale electric field, which is usually the case in the solar wind. Then by using CIS-HIA from C1 and/or C3 as reference data we find the ISR2 offsets for EFW for each of the spacecraft. We get one value for offsets per orbit.

The procedure can be controlled visually by using a plot presented in Figure 17. The two upper panels show all the available EFW and CIS-HIA data (Ex and Ey in ISR2). Then we construct the *reference E-field* from the available CIS-HIA by averaging. This is possible to do as the difference between the spacecraft in the SW/MSH is small. Then we compute the difference between the EFW Ex on all spacecraft and the reference E-field; this difference is plotted in the third panel. Average of the difference over the entire interval gives the local ISR2 offset. This offset is then applied to the EFW on different spacecraft. The resultant corrected and reference E-fields are plotted at the two bottom panels.

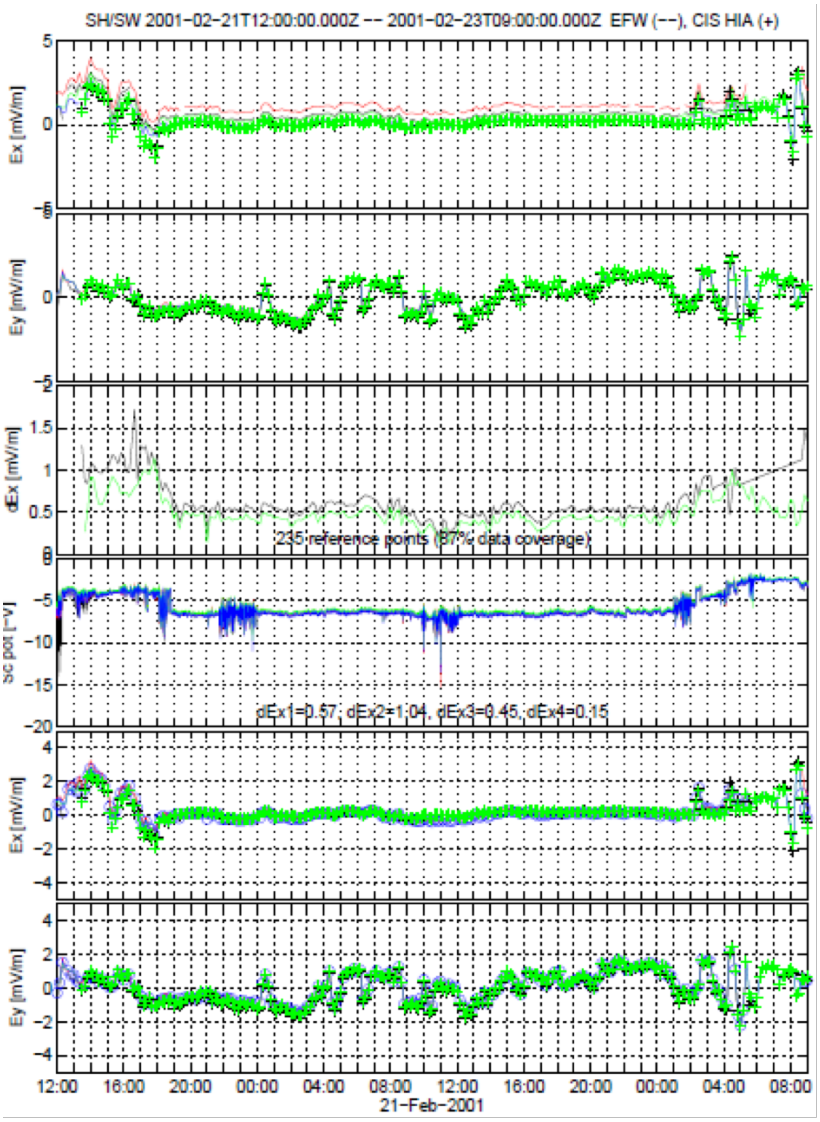

Figure 17: ISR2 offsets in the SW/MSH. The two lower panels show the electric field data to which the local offsets determined for this orbit have been applied.

We have performed this analysis for all available solar wind and magnetosheath data, grouping the data in "solar wind periods" starting in November and ending in June. Resulting ISR2 offsets for EFW on all Cluster spacecraft for 2003 are presented in Figure 18. One can see that the distribution of offsets is rather well localized near the mean value. The scatter is caused mainly by bad data and insufficient data coverage.

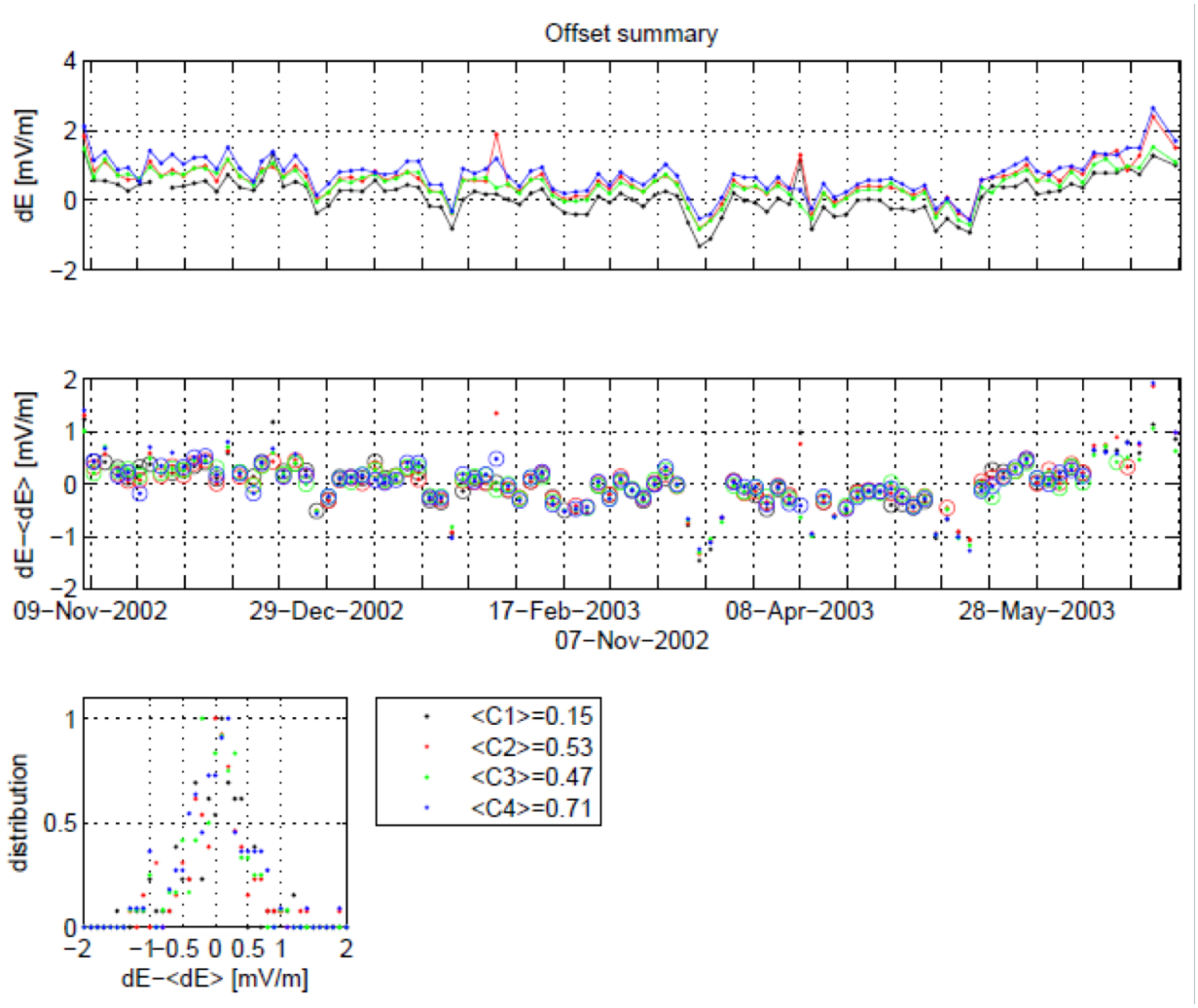

Figure 18: ISR2 offset summary (Ex) in the SW/MSH for spring 2003. The top panel shows the instantaneous offsets determined for each orbit. The middle panel shown the difference between the instantaneous offsets and the average "seasonal" offset which is used in the CAA production (<C1>..<C4> in the panel below), and which is computed on the basis of the encircled points.The distribution of the difference if shown in the bottom-left panel.

Later the offset values obtained by this automatic procedure are manually verified and if necessary corrected; the values applied are given in the FILE_CAVEATS section in the CEF files for the electric field data, for example:

```
ENTRY       =   "2007-12-02T00:00:00.000Z/2007-12-02T01:09:00.000Z
ISR2 offsets: dEx=0.85 dEy=0.00, dAmp=1.10"
```

gives the values of the ISR2 offsets and amplitude correction factor applied between 00:00

and 01:09 on 2007-12-02.

6.1.2 Offsets in the magnetosphere

The problem of determining the offsets in the magnetosphere is significantly more complicated in comparison to the solar wind/magnetosheath. Data from the other instruments which could have been used as a reference is of very low quality in large areas of the magnetosphere due to low counts or low magnetic fields (see "Cross-Calibration study"). Also the EFW data are subject to frequent problems, such as electrostatic wakes.

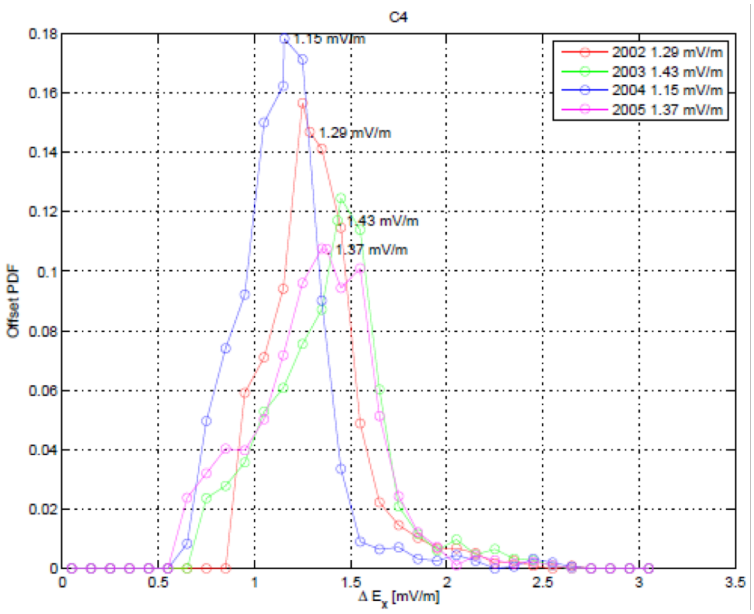

Figure 19: Summary of ISR2 X offset for Cluster 4 in the magnetosphere.

In the ISR2 offset determination procedure we decided not to use any reference data, but rather use a condition of zero electric field $<E_x>=0$, as most of the times the electric fields are really very weak in the magnetotail (X_GSE < 0 and R > 5 R_E), and averaged over a tail season this should give a rather good estimate for the ISR2 X offset.

Results for Cluster 4 are summarized in Figure 19. One can see that there is a prominent peak around 1.3 mV/m for all years, however there is also some group of points giving rise to a broadening towards lower offsets values. The nature of this broadening can be understood if we plot the ISR2 X offset against the spacecraft potential (see Figure 20). We can see a clear

cluster of points around 1.3 mV/m corresponding to the primary peak of the distribution. The main cause of broadening is due to data with ASPOC on, which can be easily identified as a cluster of point at spacecraft potential of -7 V.

In the production of the magnetospheric data we use two sets of offsets: in the dense plasma (SC potentials above -8 V) we use the "solar wind/magnetosheath" offsets and in low density plasmas we use the "magnetospheric" offsets. The values of the offsets applied together with

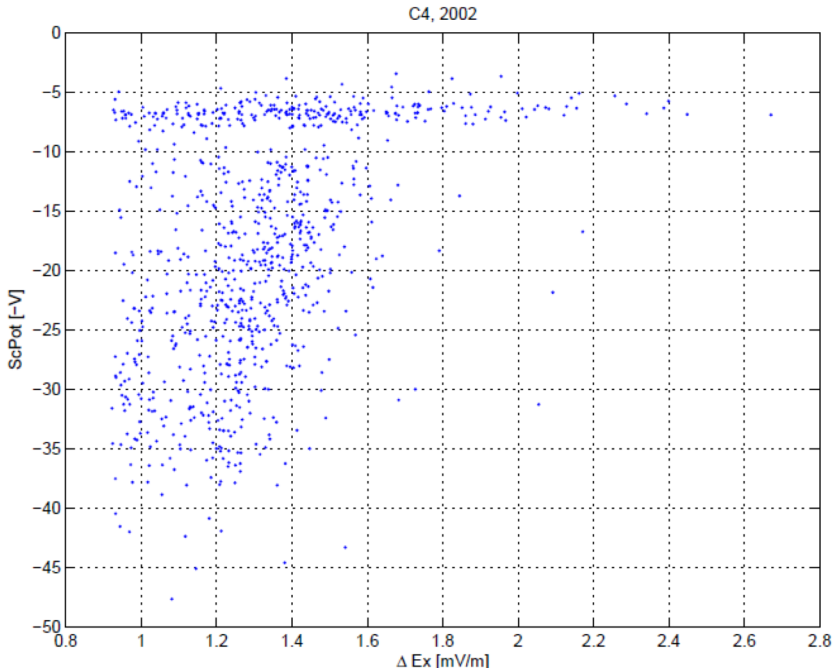

Figure 20: Sunward offset vs spacecraft potential (Cluster 4, June-November 2002).

corresponding time intervals are given in the FILE_CAVEATS section in the CEF files for the electric field data. The offsets are typically updated every several month following the spacecraft maneuvres, etc.

6.2 Comparison of E measured by EFW vs other instruments

Here we present a summary of a study comparing electric field data in the CAA measured by the EFW to EDI, CIS-HIA, CIS-CODIF and PEACE in order to evaluate the data quality resulting from the current production procedure used by the EFW team. We used 20 events covering different regions along the Cluster orbit and present electric field and convection velocity components measured by different instruments in a standard format. We conclude that EFW, as expected, provides the highest quality electric field measurements in the spacecraft spin

plane.

6.2.1 Methodology and dataset

We compare the CAA Cluster EFW measurements with those of EDI (CX_CP_EDI_MP), CIS-HIA

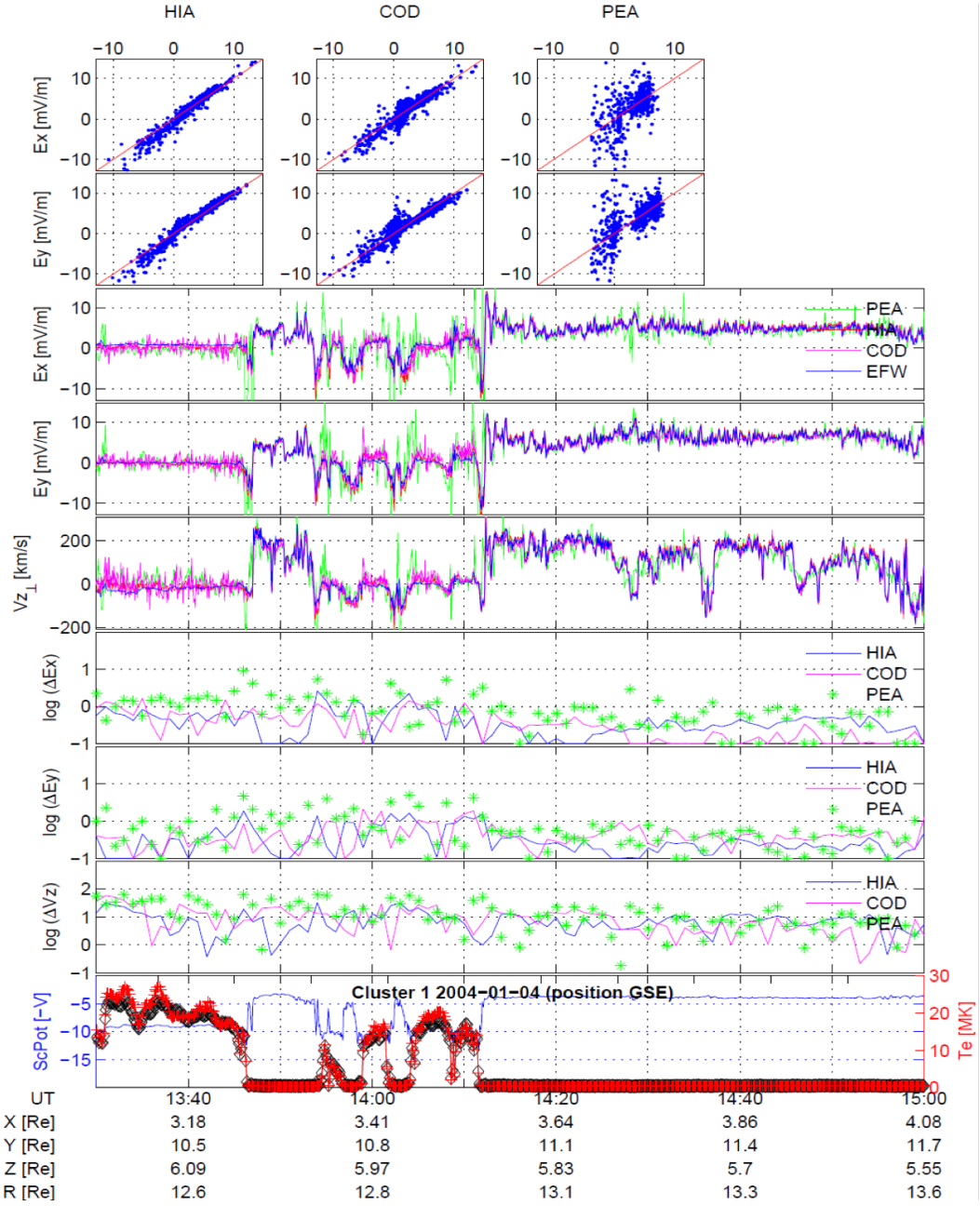

Figure 21: Cluster 1 at the magnetopause. EFW vs HIA, CODIF and PEACE.

(CX_PP_CIS,), CIS-CODIF (CX_CP_CIS-CODIF_HS_H1_MOMENTS, CX_CP_CIS-CODIF_LS_H1_MOMENTS) and PEACE (CX_CP_PEA_MOMENTS). For each event there is at least one "standard" plot with the above described data, for as many instruments as are available. For most events there are plots for both C1 and C3. C2 was not included since CIS is not operational, and C4 was not included since EDI and CIS-HIA are not operational. It should be mentioned that EFW data is routinely cross calibrated between the spacecraft and it is sufficient to show only C1 and C3.

For many events there are also "fine" plots, where one or more relevant instruments have been selected to highlight good or bad agreement. On these plots, the top three line plot panels may have a somewhat different format. The data from other instruments than EFW may be plotted as Max and Min instead of just a line plot. This Max-Min envelope of the particle instruments may be plotted in two ways, either as two lines indicating the maximum and minimum envelope of the data, or as a shaded area indicating the same thing. The color coding is given in the top panel. The envelope of the data has been calculated at 1 minute time resolution for EDI, HIA and COD, and at 4 minute time resolution for PEA.

6.2.2 Plot format

The plots contain up to 8 panels with scatter plots of data vs data at the top, followed by 7 plots of data vs time. An example plot for a magnetopause crossing is shown in Figure 21.

The scatter plots at the top are plots of EFW on the x-axis vs another instrument (EDI, HIA, COD or PEA) on the y-axis. The EFW data have been resampled to the time resolution of the other instrument. The top panel is Ex and the bottom panel is Ey. A red line through the origin with slope 1 has been included for reference.

The next three panels are line plots of Ex, Ey and Vzperp (= ExB/B^2) for all instruments available. The color coding is given in the top panel. EFW, HIA, COD and PEA are plotted as lines, while EDI is plotted as points. Each instrument is plotted with their own time resolution.

The next three panels are plots of the time-averaged (1 minute) difference between EFW and the other instruments, on a logarithmic scale. For example, the blue line shows the difference between EFW and HIA, computed as log(abs(time_average(Ex[EFW]-Ex[HIA]))). Ex and Ey are measured in mV/m, Vz is measured in km/s. The scale is 0.1-100 mV/m for E and 0.1-1000 km/s for V. The EFW data are resampled to the particle data time resolution before computing the differences. EFW-HIA and EFW-COD are plotted as lines, while EFW-PEA and

EFW-EDI are plotted as points.

The bottom panel contains for reference the spacecraft potential measured by EFW (blue) together with the electron temperature measured by PEACE (red = perpendicular, black = parallel). The spacecraft number and date is given in the bottom panel. The spacecraft coordinates below the plot are in GSE.

6.2.3 Conclusions

We have presented a comparison of the CAA EFW electric field to EDI, CIS-HIA, CIS-CODIF and PEACE. We conclude that generally EFW provides the best quality measurement of the electric field. Normally the statistical difference between the electric fields measured by EFW and other instruments lies within 1 mV/m, provided the measurements by other instruments are reasonable at all.

The observed differences between EFW and the other instruments are usually caused by higher noise and offsets in EDI and the particle instruments. However in some cases the difference may be caused by spurious fields measured by EFW, which cannot be corrected by applying offset corrections to the data.

We find that generally EFW best agrees with CIS-HIA. CIS-CODIF has much larger noise level and offset in the Z direction than CIS-HIA (especially CIS-CODIF on C3). On the other hand we find that in some cases CIS-HIA does not follow the large electric field variations which is seen by EFW, PEACE and CODIF. We also found cases when HIA and CODIF data differ by a constant factor.

We find that PEACE moments have very limited use inside the magnetosphere. However, there is a good agreement between EFW and PEACE in the magnetosheath, especially when the SC is in the burst mode.

EFW-EDI comparisons in some cases show a remarkable agreement down to 0.1 mV/m for quiet fields. However, in more active regions EDI has much more scatter, which is expected. In general the agreement between EFW and EDI is very good.

Finally, we conclude that we see the expected picture: the quality of the electric field measured by the different instruments strongly depends on the plasma environment. We usually find a statistical agreement between EFW and at least one of the other instruments within 1 mV/m. Provided that the measured field is real, EFW generally provides the best measurement of the electric field. The production procedure used by the EFW team results in

high data quality.

More information about this study can be found in "Cross-Calibration study", see references.

7 Summary

Processing of EFW data for the CAA is a complex procedure which requires a number of calibration and cross-calibration steps at which different offsets are determined.

7.1 Raw data and calibration parameters

The calibration parameters determined during the data processing as well as some instrument settings values and raw data signals are available as ancillary datasets (for details, see The ICD).

Sampling rate	CAA Dataset name	Description
5 s^{-1}	C[n]_CP_EFW_L1_P1	Potential, Probe 1 to spacecraft (raw data)
	C[n]_CP_EFW_L1_P2	Potential, Probe 2 to spacecraft (raw data)
	C[n]_CP_EFW_L1_P3	Potential, Probe 3 to spacecraft (raw data)
	C[n]_CP_EFW_L1_P4	Potential, Probe 4 to spacecraft (raw data)
25 s^{-1} or 450 s^{-1}	C[n]_CP_EFW_L1_P12	Potential, Probe 1 to Probe 2 (raw data)
	C[n]_CP_EFW_L1_P32	Potential, Probe 3 to Probe 2 (raw data)
	C[n]_CP_EFW_L1_P34	Potential, Probe 3 to Probe 4 (raw data)
0.25 s^{-1}	C[n]_CP_EFW_L3_DER	Electric Field offsets (4 second resolution)
0.25 s^{-1}	C[n]_CP_EFW_L3_SFIT	Spinfits of the electric field from the individual probe pairs
1/32 s-1	C[n]_CP_EFW_L2_HK	Instrument settings

The Level 1 datasets (first 7 rows above) are the ***raw data*** from the instrument, decommutated and converted to physical units. **P1**, **P2**, **P3**, **P4** are the potentials of the four individual probes, measured relative to the spacecraft. **P12**, **P34** and **P32** are potential differences between pairs of probes. Notice that the spacecraft attitude and orbit parameters as well as the sun reference pulse all needed for the interpretation of raw signal are given in the CAA spacecraft auxiliary datasets (see Laakso, 2011).

C[n]_CP_EFW_L3_DER is the DC offset in the raw data. See section 6.1 for more information. DER is a vector with 2 components and, depending on which probes are available for E-field measurements, contains either the offsets in p12 and p34 or the offsets in p32 and p34.

7.2 Long-term evolution of offsets

Figure 22 shows evolution of Delta offsets (difference between ISR2 E measured by probe pairs 12/32 and 34). Variations in the offset are caused by a number of factors. First is the solar cycle. One can see that the offset is rather small and steady in the beginning of the mission and starts to grow with approach of the solar minimum, reaching it's maximum in spring 2006. This behavior is caused by non-optimal bias current settings, and the situation

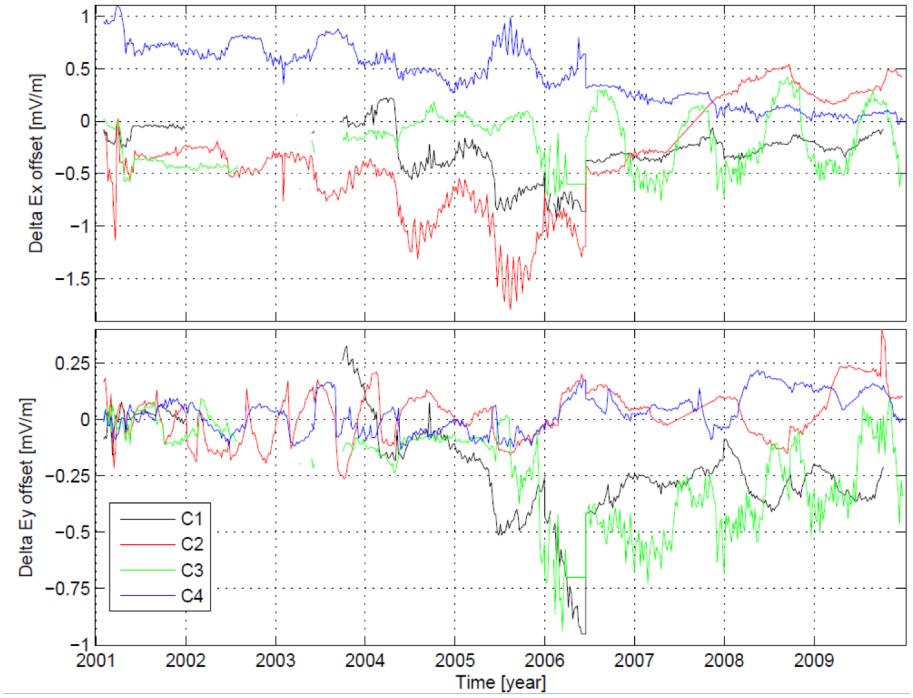

Figure 22: Evolution of delta offsets

was significantly improved by lowering the bias current in June 2006. The second cause is the probe failures which forced usage of P32 instead of P12. P32 has lower quality as it is not symmetric with respect to the spacecraft.

Evolution of ISR2 (DSI) offsets in the solar wind and magnetosheath during mission lifetime is shown in Figure 23. One can see that the offsets are rather steady and slowly decreasing with approach of the solar minimum (~2009). The only striking feature is the sudden increase of the offset on C3 in 2005. This change is not yet understood.

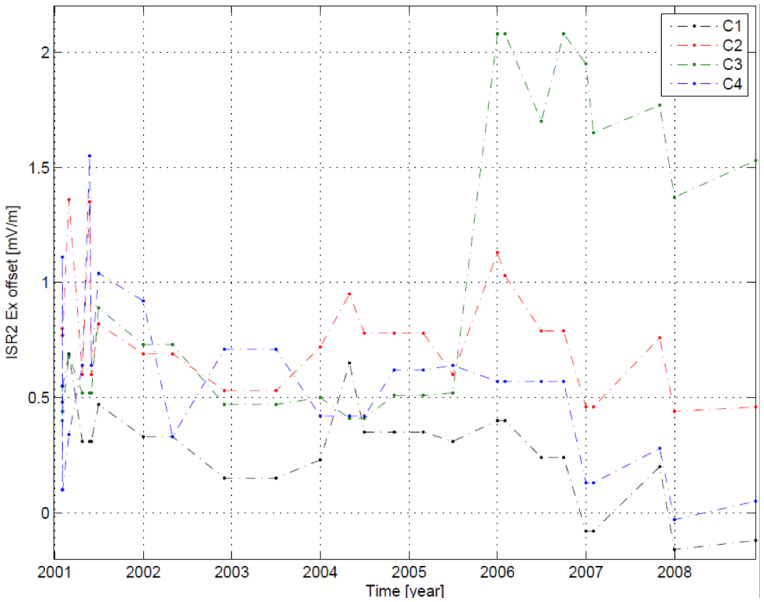

Figure 23: Evolution of ISR2 (DSI) offsets in the SW/MSH

Evolution of ISR2 offsets in the magnetosphere during mission lifetime is shown in Figure 24. The offsets are steady and slowly decreasing with approach of the solar minimum.

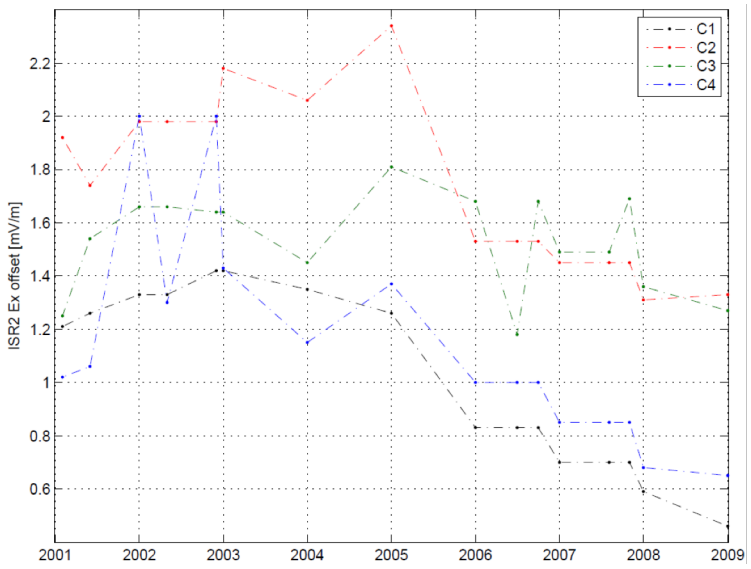

Figure 24: Evolution of ISR2 (DSI) offsets in the magnetosphere

8 References

EFW Standard operations database (http://www.cluster.irfu.se/efw/ops/#standard_table)
EFW "non-standard operations" database (http://www.cluster.irfu.se/efw/ops/ns_ops.html)

Cross-Calibration study EFW vs others (http://www.cluster.irfu.se/efw/efw_vs_others/)

Cully C. M., R. E. Ergun, and A. I. Eriksson, Electrostatic structure around spacecraft in tenuous plasmas, J. Geophys. Res. 112, A09211 (2007). doi:10.1029/2007JA012269

Gustafsson, G., R. Boström, B. Holback, G. Holmgren, A. Lundgren, K. Stasiewicz, L. Åhlén, F. S. Mozer, D. Pankow, P. Harvey, P. Berg, R. Ulrich, A. Pedersen, R. Schmidt, A. Butler, A. W. C. Fransen, D. Klinge, M. Thomsen, C.-G. Fälthammar, P.-A. Lindqvist, S. Christenson, J. Holtet, B. Lybekk, T. A. Sten, P. Tanskanen, K. Lappalainen, and J. Wygant, The Electric Field and Wave Experiment for the Cluster Mission, Space Sci. Rev. 79, 137-156 (1997)

Engwall, E., A. I. Eriksson, and J. Forest, Wake formation behind positively charged spacecraft in flowing tenuous plasmas, Phys. Plasmas 13, 062904 (2006). doi: 10.1063/1.2199207

Eriksson, A. I., M. André, B. Klecker, H. Laakso, P.-A. Lindqvist, F. Mozer, G. Paschmann, A. Pedersen, J. Quinn, R. Torbert, K. Torkar, and H. Vaith, Electric field measurements on Cluster: comparing the double-probe and electron drift techniques, Ann. Geophys. 24, 275-289 (2006)

Eriksson, A. I., Y. Khotyaintsev, and P.-A. Lindqvist, Spacecraft wakes in the solar wind, In Proceedings of the 10th Spacecraft Charging Technology Conference (SCTC-10), (2007) URL : http://www.space.irfu.se/aie/publ/Eriksson2007b.pdf

Laakso, H. Cluster Active Archive – User Guide, CAA-EST-UG-0001, (2011). (https://caa.esac.esa.int/documents/UG/CAA-EST-UG-0001-v10.pdf)

Lindqvist, P.-A. and Y. Khotyaintsev, Cluster Active Archive: Interface control document for EFW, ESA document CAA-EFW-ICD-0001 (2013),
URL : https://caa.esac.esa.int/caa/ug_cr_icd.xml

Lindqvist, P.-A., C. M. Cully and Y. Khotyaintsev, User Guide to the EFW measurements in the Cluster Active Archive (CAA), ESA document CAA-EST-UG-EFW (2013),
URL : https://caa.esac.esa.int/caa/ug_cr_icd.xml

Puhl-Quinn, P. A., H. Matsui, V. K. Jordanova, Y. Khotyaintsev, and P.-A. Lindqvist, An effort to derive a convection electric field model in the inner-magnetosphere: Merging Cluster EDI and EFW data, J. Atmosph. Solar-Terr. Phys., 70, 564-573 (2008). doi: 10.1016/j.jastp.2007.08.069

Shue, J.-H., J. K. Chao, H. C. Fu, C. T. Russell, P. Song, K. K. Khurana, and H. J. Singer, A new functional form to study the solar wind control of the magnetopause size and shape, J. Geophys. Res., 102, 9497-9512, (1997). doi: 10.1029/97JA00196